

ELM mitigation by nitrogen seeding in the JET Gas Box Divertor

J. Rapp[†], T. Eich[†], M. von Hellermann[‡], A. Herrmann[¶], L.C. Ingesson[‡], S. Jachmich[§], G.F. Matthews^{||}, V. Philipps[†], G. Saibene^{II} and contributors to the EFDA-JET workprogramme[#]

[†]Institut für Plasmaphysik, Forschungszentrum Jülich GmbH, EURATOM Association, Trilateral Euregio Cluster, Jülich, Germany.

[‡]FOM Instituut for Plasmafysica Rijnhuizen, EURATOM Association, Nieuwegein, The Netherlands.

[¶]Max-Planck Institut für Plasmaphysik, EURATOM Association, Garching, Germany.

[§]ERM/KMS, EURATOM Association, Brussels, Belgium.

^{||} UKAEA/Fusion Association, Culham Science Center, Abingdon, OXON, UK.

^{II} EFDA Home Team, Garching, Germany.

Abstract. One of the most severe problems for fusion reactors is the power load on the divertor target plates. Technically only power loads of less than 10 MW/m^2 are acceptable. However, strong ELM (Edge Localized Mode) activity can lead to power loads in excess of 800 MW/m^2 . In order to reduce the steady-state heat flux and the transient heat flux due to ELMs radiative cooling experiments were performed at JET. Nitrogen was puffed into the divertor up to a radiative power fraction of 90%. This was achieved at a density of 0.85 times the Greenwald density [1], while maintaining an H-factor of $f_{H98} = 0.82$. The Z_{eff} in all those discharges stayed around 2.0. At approximately 55% radiative power fraction the ELM characteristic changes from type-I to type-III, resulting in a loss of confinement of about 25% due to a degradation of the edge pedestal and hence a reduction of the ELM power load to the divertor tiles. By increasing the radiative power fraction to values of about 90% the heat flux is further reduced to 2 MW/m^2 although the stored energy is increasing.

[#] see appendix of the paper by J. Pamela *Overview of recent JET results*, Proceedings IAEA Conference on Fusion Energy, Sorrento, 2000

1. Introduction

Radiation cooling experiments with extrinsic impurities have been performed on several tokamaks [2, 3, 4] in order to reduce the heat flux to the plasma facing components such as limiters or divertors. For ITER average steady state heat fluxes below 10 MW/m^2 have to be obtained, which requires a very shallow angle of incidence or cooling due to radiation. Due to the strong transient heat loads, type-I ELMy H-modes are eventually unacceptable as an operating scenario for ITER. The solution to the problem of transient heat loads might be the operation in H-modes with type-II ELMs or small type-III ELMs.

Additionally to the reduction of the transient heat loads a reduction of the temperature in front of the divertor target below 10 eV is necessary in order to be compatible with the application of a tungsten divertor, which erosion yields due to the impact of light impurities drop drastical below 10 eV . For those reasons it has to be demonstrated that an operation with a partial detached divertor and target temperatures of several eV is feasible. Extensive studies on Nitrogen seeded discharges in the JET Mk-I, Mk-IIA and Mk-IIAP divertors have been reported by *Matthews et al.* [4]. In this article the application of Nitrogen seeding within a type-III ELMy H-mode scenario in the closed JET gas box divertor Mk-IIGB is studied. The JET Mk-IIGB is the most closed one in a series of divertor, which were tested at JET. In figure 1 all JET divertors are displayed. This "gas box" type geometry and the vertical targets are also foreseen for ITER.

2. Radiation cooling by nitrogen seeding in the JET gas box divertor

At JET many impurity seeding experiments have been performed [4, 5]. In this article experiments with nitrogen seeding are reported. Nitrogen is a low- Z impurity, which has its maximum in the cooling rate (coronal equilibrium) at $\approx 10 \text{ eV}$. Hence it is radiating at these low temperatures which are typical in the divertor. At temperatures above 2 keV it is totally ionized, thus leading to little radiation from the plasma core. Furthermore nitrogen is a non-recycling gas, which will minimize migration from the divertor region to the main chamber region. Indeed it was shown that increasing the Z by using neon or argon instead of nitrogen the ratio of the divertor radiation to the bulk radiation is decreasing [4]. This altogether gives hope that nitrogen is optimal to localize the radiation in the divertor without influencing the plasma core too much.

In figure 2 an overview of a typical discharge (2.5 MA , 2.4 T , high clearance equilibrium, vertical target) is shown (#53318). Deuterium and nitrogen are fueled with $\Gamma = 3 \times 10^{22} \text{ e/s}$. At a radiative power fraction of 55% the ELM characteristic changes from type-I to type-III ELMs. At the same time the confinement drops from $f_{H98} = 1.0$ to $f_{H98} \approx 0.8$. The Z_{eff} is increasing for the duration of the seeding up to 2.1 . At 19.5 s the total radiative power reaches its peak-value (90%). Most of the radiation originates from the X-point region in this detached case as the tomographic reconstructions show (fig. 3), whereas in the attached case significant radiation is also encountered from the vicinity of the target plates. During the whole discharge

regular sawtooth activity is observed and no accumulation of nitrogen on axis was encountered, as the hollow nitrogen concentration profile at the highest radiation level demonstrates (fig. 4).

3. Power Balance

In order to proof the effect of radiation cooling, it has to be shown that the thermal load on the divertor tiles is indeed significantly reduced. For pulse #53318, in which a maximum radiated power fraction of 90% was achieved an energy balance was performed by balancing the input energy with the radiated and convected energy ($W_{in} = W_{rad} + W_{conv}$) during the diverted discharge phase. The total radiated energy is determined by the bolometers. The convected energy is derived by the divertor thermo-couples and taking into account the absorption of radiated energy on the divertor tiles ($W_{rad,div}$). The ratio between the power radiated onto the divertor tiles $P_{rad,div}$ and the total radiated power P_{rad} is derived from tomographic reconstructions of the multi-chord bolometer diagnostic. After the local emissivity is obtained, the wall load of each individual wall segment is calculated taking into account the full geometry of the vacuum vessel. In order to minimize the effect of uncertainties in the divertor region, resulting from very local radiation zones, the heat load due to electromagnetic radiation is integrated over all divertor tiles. The JET divertor is equipped with 22 thermo-couples from which the total absorbed energy on the divertor tiles for a complete discharge is derived ($W_{div} = W_{conv} + W_{rad,div}$). A remarkable agreement is found for the energy W_{div} derived from thermo-couples (67.6 MJ) and derived from the input energy and radiated energy (67.4 MJ), indicating that those high radiative power fractions are reliable.

For a more detailed power balance IR thermography is necessary. Since the thermography system in the JET gas box divertor has a complicated periscope view and the septum is vignetting large fractions of divertor region, not all configurations are suitable for a reliable measurement. For this reason a configuration with upward shifted strike zones has been chosen in order to optimize the IR-thermography analysis [6]. In such an optimized configuration (#53772) a power balance has been made. Nitrogen is seeded up to a total radiated power fraction of 80%. The temporal evolution of the heating power (P_{heat}), the change in the stored energy (dW_{dia}/dt), the total radiated power onto the main chamber walls ($P_{rad,bulk} = P_{rad} - P_{rad,div}$, as derived from tomography) and the total heat flux on the divertor tiles (P_{div}) derived from thermography is shown in figure 5. In general the power balance $P_{bal} = P_{heat} - P_{rad,bulk} - P_{div} - dW_{dia}/dt$ is consistent in the period from 18 sec to 25 sec within the experimental error bars. A principle deviation occurs in the beginning of the auxiliary heated discharge period. Here, 3 MW are missing in the balance. There are uncertainties in the determination of the total heat load onto the divertor tiles, since a large fraction of the inner baffle is not covered by the IR-thermography system. A further uncertainty is the background radiation from the periscope system of the IR-system when the surface temperature is low, as it is the case in the beginning of a diverted discharge. The supposition of missing divertor power load is emphasized when the IR thermography data are compared to the divertor

thermo-couples. On divertor tiles away from the actual strike zones the energy derived from thermography is systematic lower than the energy derived from the thermocouples. The error of 15% in the radiated power after tomographic reconstruction cannot explain the discrepancy of 3 MW.

4. ELM mitigation

In the previous section it was shown that the total power flux to the divertor target can be reduced significantly. Nevertheless, the essential question with respect to the success of the radiation cooling is related to the ELM power deposition. Is it possible to actually buffer ELMs by the gas target or radiate large fractions of the ELM energy before hitting the target? Furthermore, is it possible to reduce the electron temperature in front of the target plate also transiently during ELMs below 10 eV?

Unfortunately, due to technical reasons (vignetting effects in the Mk-IIIGB divertor), good measurements with the IR thermography and measurements with the fixed Langmuir probes are mutually exclusive. Due to this reason the information on ELMs from Langmuir probe measurements is extracted from pulse #53318 (max. 90% radiation) and for the IR thermography pulse #53772 (max. 80% radiation) is used.

For JET a general approach for the characterization of the divertor detachment was developed [7, 4]. This criterion, degree of detachment (DoD), compares the expected ion saturation current I_s^{scal} for attached conditions, as derived from a simple 2-point model, with the actual measured ion saturation current I_s^{meas} . When the deviations between both are larger than certain values, the divertor is detached. The expected ion saturation current scales like $I_s^{scal} \propto \bar{n}_e^2 / (1 - f_{rad})$, with f_{rad} being the radiative power fraction. If the $DoD = I_s^{scal} / I_s^{meas}$ is larger than 2 for the peak ion flux or larger than 10 for the integrated ion flux the divertor is considered to be completely detached [7]. It is important to note that for the high frequent type-III ELMs present here the time in between ELMs is with 3 ms (see also fig. 7) significantly larger than the particle dwell time in the SOL with 0.4-1 ms. This means that the SOL is equilibrated in between ELMs, which is a pre-requisite for the application of the 2-point model in the conduction-limited regime.

The steady state of the divertor is determined by the particle and heat flux in-between ELMs. The DoD, as derived from the lower envelope of the ion saturation current (I_s), is shown in figure 6. When the H-mode plasma has type-I ELMs the divertor is attached. After the transition from type-I ELMs to type-III ELMs the DoD^{peak} becomes 10 and the integrated DoD^{int} becomes 20 at the inner divertor. At the strike point of the outer divertor the DoD as well reaches values ≥ 6 . This means that as soon as type-III ELMs are present at least the inner divertor is completely detached in-between ELMs.

The picture is more complicated during the actual ELM event. Figure 7 shows the upper envelope of the ion saturation current at the outer strike zone I_s , meaning the amplitude of the ELMs, and the ELM frequency. By increasing the radiation level the amplitude of I_s is decreasing while the ELM frequency is increasing up to 300 Hz. The product of ELM frequency

and ELM amplitude is slightly decreasing. However, the electron temperature in front of the target plate is decreasing strongly with increasing radiation level. At the highest level of radiation during the type-III ELMs the peak electron temperature, measured in front of the target plate, is reduced to 10 eV. This is a successful demonstration of the radiation cooling. From the Langmuir probes also the parallel heat flux density can be derived: $q_{\parallel} = j_s(7.8T_e + E_{rec})$, with $E_{rec} = 17.8\text{eV}$ being the ionization energy (13.6 eV) and the recombination energy (4.2 eV) of the deuterons which recombine to molecules at the wall. In order to be comparable to IR-measurements this parallel heat flux is recalculated into a perpendicular heat flux to the target surface flux by taking into account the pitch angle of the field line to the target plate (fig. 8). The peak heat flux density (during ELMs, upper envelope) is reduced during the highest radiative power fractions down to $P_{target} \approx 2 \text{ MW/m}^2$. This is in good agreement with IR-thermography measurements (figure 9), which have been taken in a similar pulse (#53772). This strong reduction in the power flux to the target (approx. factor 3) is not consistent with a scaling $\Delta W_0 = P_{in}/f_{ELM}$, with ΔW_0 being the energy lost by an ELM, introduced by *Fishpool* [8], since the ELM frequency is only moderately raising (approx. factor 1.5). This seems to be an indirect indication of ELM mitigation.

However, under ELM mitigation one understands primarily the reduction of the heat flux from the pedestal to the target plates during the ELM event. A proof of this is only possible by a comparison of the $\Delta W_{dia}/W_{dia}$ dependence and the P_{target} dependence. The ELM band (area between upper and lower envelope) in the power flux density measured by the IR-thermography at the divertor target is reduced indicating ELM mitigation. But this could have the trivial reason that the energy lost in the pedestal region of the plasma is decreasing as well. The analysis of the fast diamagnetic energy signal does not resolve this problem. The ELM amplitude is lower than the noise level of the signal (100 kJ) and the inter ELM time is in the similar range as the characteristic time of the presence of eddy currents, which disturb the measurement. Another way determining the energy loss by ELMs is measuring the kinetic energy loss in the plasma. By taking the electron temperature at the pedestal (ECE channel here at $R = 3.685 \text{ m}$) and the line-averaged density from an interferometer channel crossing the pedestal region the kinetic electron energy can be deduced. This method is in detailed described in [8]. The total energy loss per ELM derived is $\Delta W/W \approx 0.7\%$ with an ELM-frequency of $\approx 100 \text{ Hz}$ (#53772, $t = 23.4 \text{ s}$). Those values are in the range of other type-III ELM losses in discharges with impurity seeding [4, 5]. However, the error bar in the determination of the kinetic energy loss is large due to the uncertainties in the assumptions about the relative contributions of electrons and ions as well as geometric uncertainties in the pedestal location. Hence, more detailed and more precise investigations in this respect are required in order to proof if nitrogen seeding leads to ELM mitigation.

5. Comparison of the Mk-II gas box divertor to the more open divertors with respect to nitrogen seeding

In the previous sections it was shown that an operation with a partially detached divertor is possible in the closed Mk-II gas box divertor. Energy and power balances are consistent, thus confirming the feasibility of type-III ELMy H-mode scenarios with about 90% radiative power fraction. The intention of the closed Mk-IIIGB (installed in 1998) was to increase the divertor radiation with respect to the total radiation and to reduce the plasma core pollution with extrinsic impurities. For this reason it is useful to compare the results obtained in the JET MK-IIIGB with the more open predecessors: the very open Mk-I (1994-1996), the more closed Mk-IIA and Mk-IIAP with plugged leakage paths (1996-1998). For the characterization of all divertors an improved, consistent estimate of the total radiated power, based on tomographic reconstructions, is used. In order to minimize errors due to reconstruction artefacts in the divertor region and to increase reliability not all divertor bolometer channels are used for the evaluation of the total radiated power within this algorithm. This algorithm was cross validated by an energy balance with thermo-couple data in the Mk-IIIGB divertor. A thorough re-evaluation of the total radiated power in nitrogen discharges has been made for all JET divertors, including the discharges in *Matthews et al.* [4].

Figure 10 shows for all divertors the maximum achieved radiated power fraction versus the ratio of divertor to bulk radiation. Note: this ratio does not distinguish between radiation from divertor legs and radiation from the X-point region. First of all, increasing the radiative power fraction by seeding of nitrogen leads to an increased divertor radiation. This dependence is linear regardless of the divertor closure. Of course this does not mean that the radiation in the divertor legs is increased. As it was shown in section 2 with increasing radiative power fraction the peak of the radiation distribution moves towards the X-point region leading also to enhanced radiation inside the LCFS. This is similar to all other divertors [4]. The highest radiative power fraction was achieved in the Mk-I. Mk-IIA data are systematically lower than Mk-I and Mk-IIIGB data. For Mk-IIAP unfortunately only data from disrupted discharges were available. All the data from the disrupted discharges reveal the same linear dependence, but lead to an even larger scatter of the data. This scatter mainly reflects different machine operating areas, but does not reveal an operating boundary. This seems to suggest that the divertor closure has no effect on the maximum achievable radiative power fraction. Furthermore, there are strong indications that in several of the disruptive nitrogen seeded discharges the radiative power fraction just before the disruption is about 100%. This suggests that the actual limit for those radiating scenarios is the radiative collapse, which is a global limit not depending on divertor geometry. More investigations at the H to L-mode boundary are necessary to be able to give a clear answer to the operational limit of those radiation cooled discharges.

Previous conclusions [4], based on a power balance between bolometer data and Langmuir probe data, have to be modified somewhat. When comparing the maximum achieved radiative power fractions, derived by the new algorithm, for the Mk-I divertor (#33204), with the results of the old analysis published in [4], it is obvious that less neutral particle loss is needed to be

Table 1. Effect of divertor closure on detachment process; DoD at inner divertor.

Divertor	f_{rad} (DoD ^{int} \geq 10)	N^{GW} (DoD ^{int} \geq 10)	DoD ^{max}
Mk-I	85	70	10
Mk-IIA	65	65	20
Mk-IIAP	60	65	40
Mk-IIIGB	55	65	100

assumed to achieve a consistent power balance. The previously assumed high level of neutral particle loss was not supported by EDGE2D/NIMBUS simulations in conjunction with more-detailed bolometer analysis anyway [9]. So, it seems that the neutral particle loss is non-significant and can be neglected in the power balance for those highly radiating nitrogen seeded discharges.

As previously noted [4], the detachment becomes more pronounced as the divertor becomes more closed. The radiative power fraction at the onset of complete detachment (DoD^{int} \geq 10) is decreasing with increasing divertor closure (see table 1). Similarly the maximum achieved degree of detachment is increasing significant with increasing divertor closure. Though, the onset of the detachment with respect to the Greenwald number $N^{GW} = \bar{n}_e/n_e^{GW}$ is unaffected by the divertor closure.

6. Conclusions

It has been shown that a radiation cooling scenario with radiative power fractions of more than 90% is possible at JET, regardless of the divertor closure. This type-III ELMy regime leads to a partially detached H-mode at 85% of the Greenwald density and H-factors of $f_{H98} = 0.82$. The heat flux density is reduced to about 2 MW/m² and electron temperatures in the divertor of less than 10 eV are feasible. No clear conclusion on the type-III ELM mitigation could be drawn. More detailed investigations in this respect are required. There is potential to increase the operational range of this scenario to higher densities by increasing the triangularity. The discharges shown in this paper had triangularities of $\delta \approx 0.2$. Furthermore, there is potential to increase the confinement by lowering the safety factor at the edge. Altogether this could be an ITER scenario for Q= 10 with $f_{H98} = 0.82$ and $\bar{n}_e/\bar{n}^{GW} = 1.0$ and an edge safety factor of $q_{95} = 2.6$.

7. References

- [1] Greenwald M *et al* 1988 Nucl. Fusion **28** 2199
- [2] Samm U *et al* 1993 Plasma Phys. Control. Fusion **35** B167
- [3] Kallenbach A *et al* 1995 Nucl. Fusion **35** 1231
- [4] Matthews G F *et al* 1999 Nucl. Fusion **39** 19

- [5] Strachan J D *et al* 2000 *Plasma Phys. Control. Fusion* **42** A81
- [6] Eich T *et al* 2001 *Proc. 28th European Physical Society Conf. on Controlled Fusion and Plasma Physics (Funchal, 16-23 June 2001)*
- [7] Loarte A *et al* 1998 *Nucl. Fusion* **38** 331
- [8] Fishpool G M 1998 *Nucl. Fusion* **38** 1373
- [9] Ingesson L C 1997 *Proc. 24th European Physical Society Conf. on Controlled Fusion and Plasma Physics (Berchtesgaden, 9-13 June 1997) Europhys. Conf. Abstr. vol. 21a, Part I, ed M Schittenhelm, R Bartiromo and F Wagner (Geneva: European Physical Society) p 113*

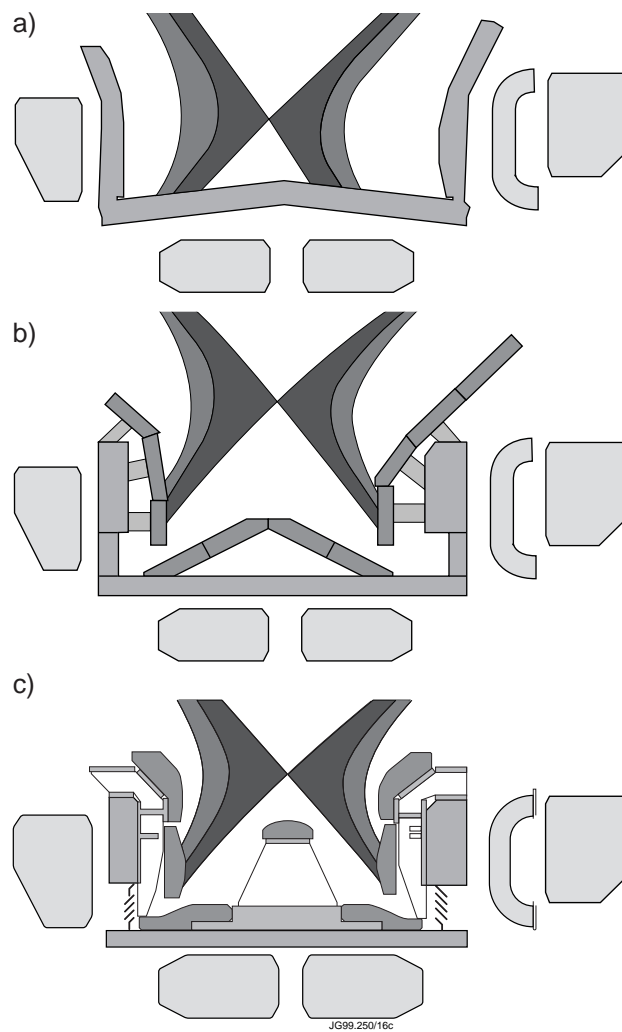


Figure 1. JET divertors: a) Mk-I; b) Mk-IIA; c) Mk-IIGB.

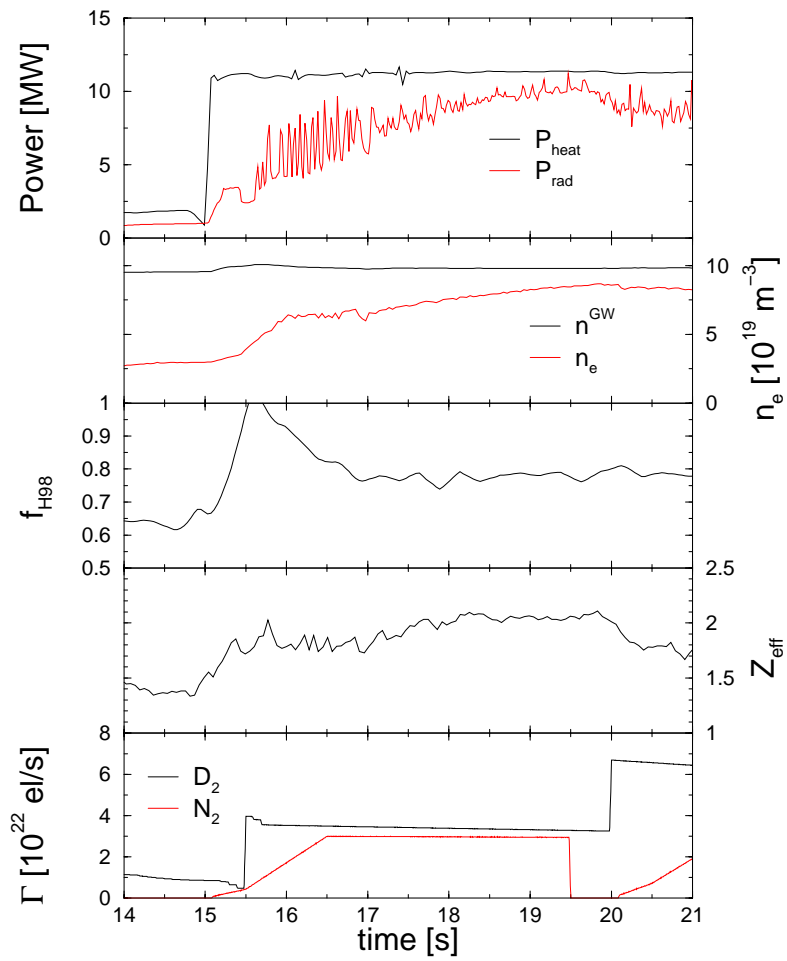


Figure 2. #53318: overview over discharge; $I_p = 2.5$ MA, $B_t = 2.4$ T, $\delta = 0.2$, high clearance equilibrium, vertical target.

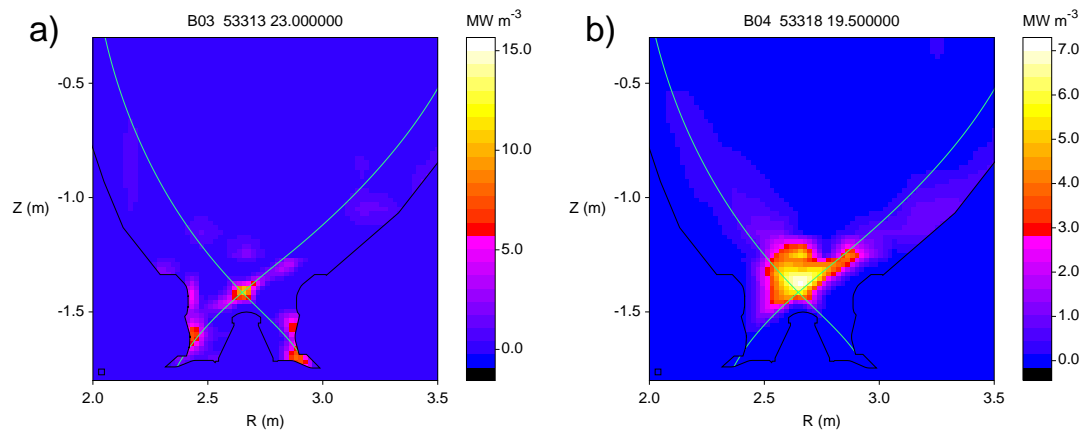


Figure 3. Tomographic reconstructions of the total radiated power derived from bolometry; a) #53313, 23 s: attached divertor conditions with type-I ELMs, averaged over type-I ELMs, 40% radiative power fraction; b) #53318, 19.5 s: detached divertor conditions with type-III ELMs, averaged over type-III ELMs, 90% radiative power fraction.

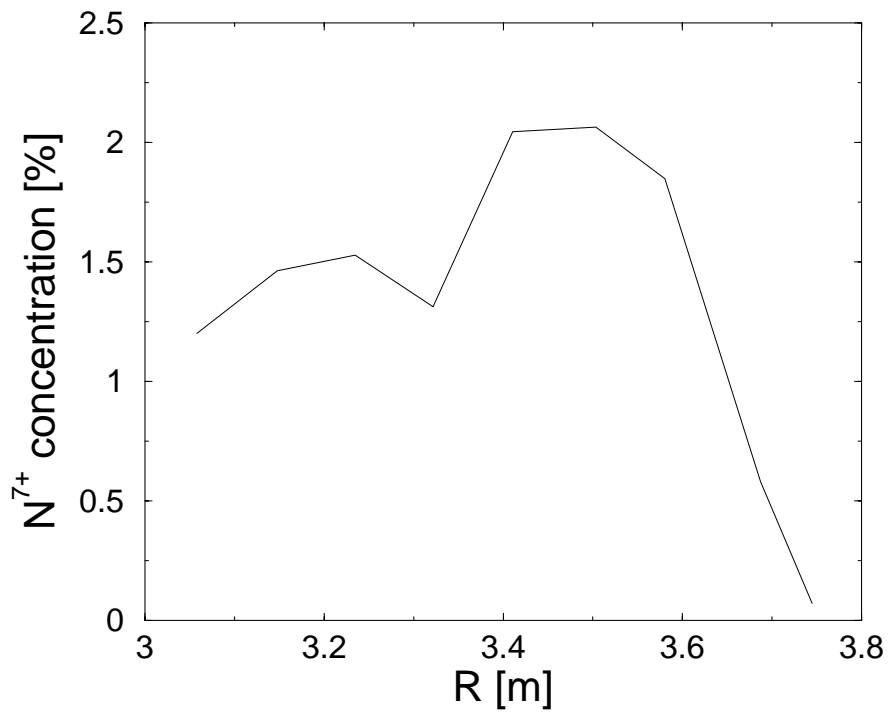


Figure 4. #53318, $t=19.5$ s: nitrogen concentration profile as derived from CXRS.

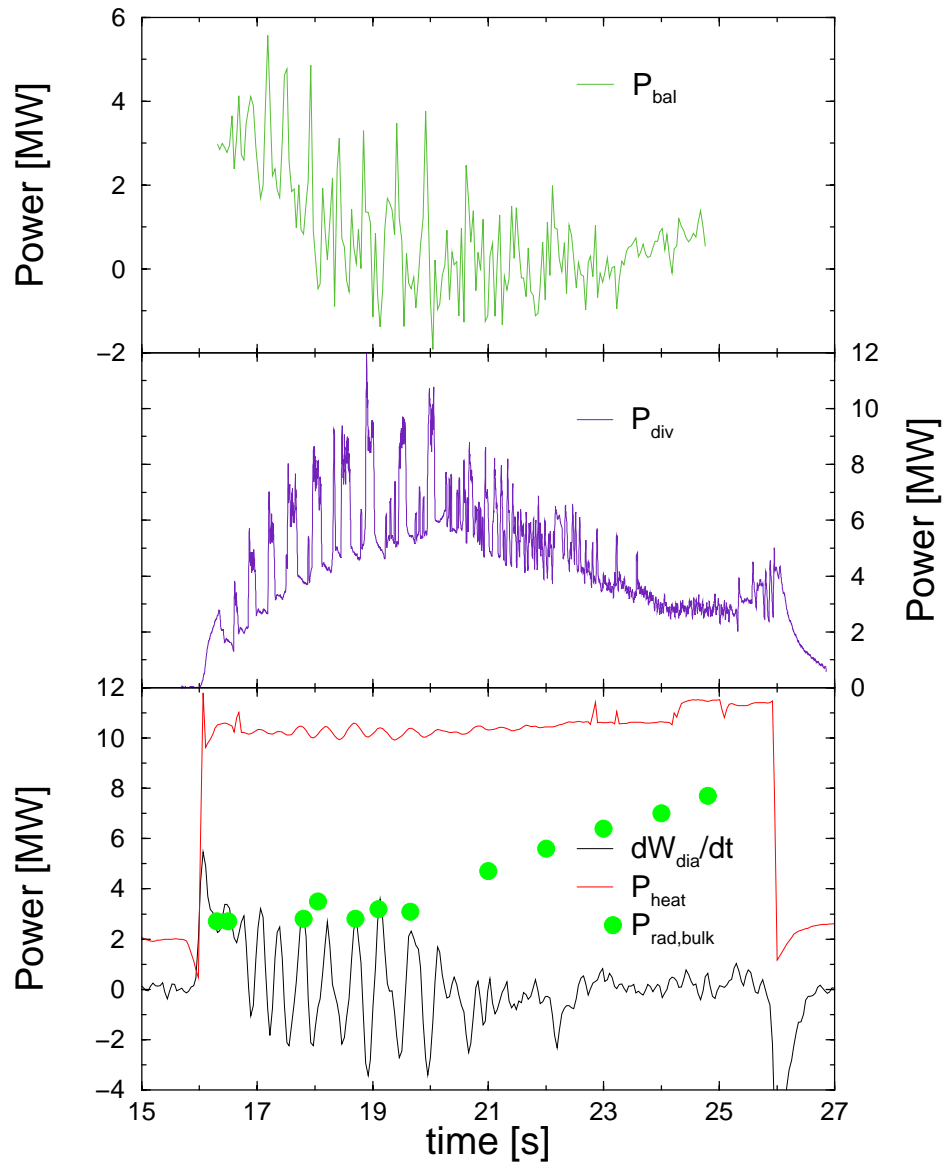


Figure 5. #53772: Power balance P_{bal} as derived from IR-thermography P_{div} , bolometric reconstructions $P_{rad,bulk}$, heating power P_{heat} and the change in diamagnetic energy dW_{dia}/dt ; $P_{bal} = P_{heat} - P_{div} - P_{rad,bulk} - dW_{dia}/dt$.

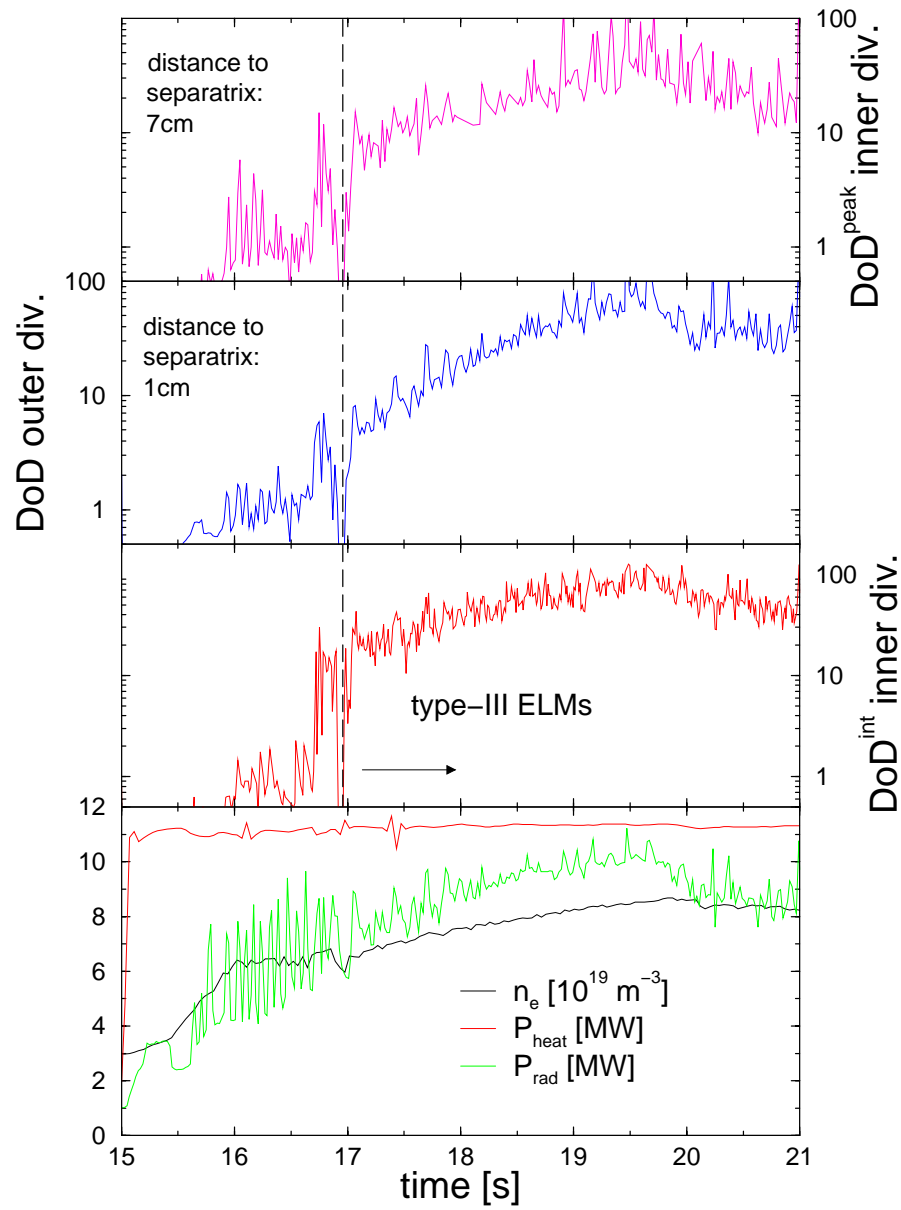


Figure 6. #53318: Degree of detachment (DoD) at inner and outer divertor target.

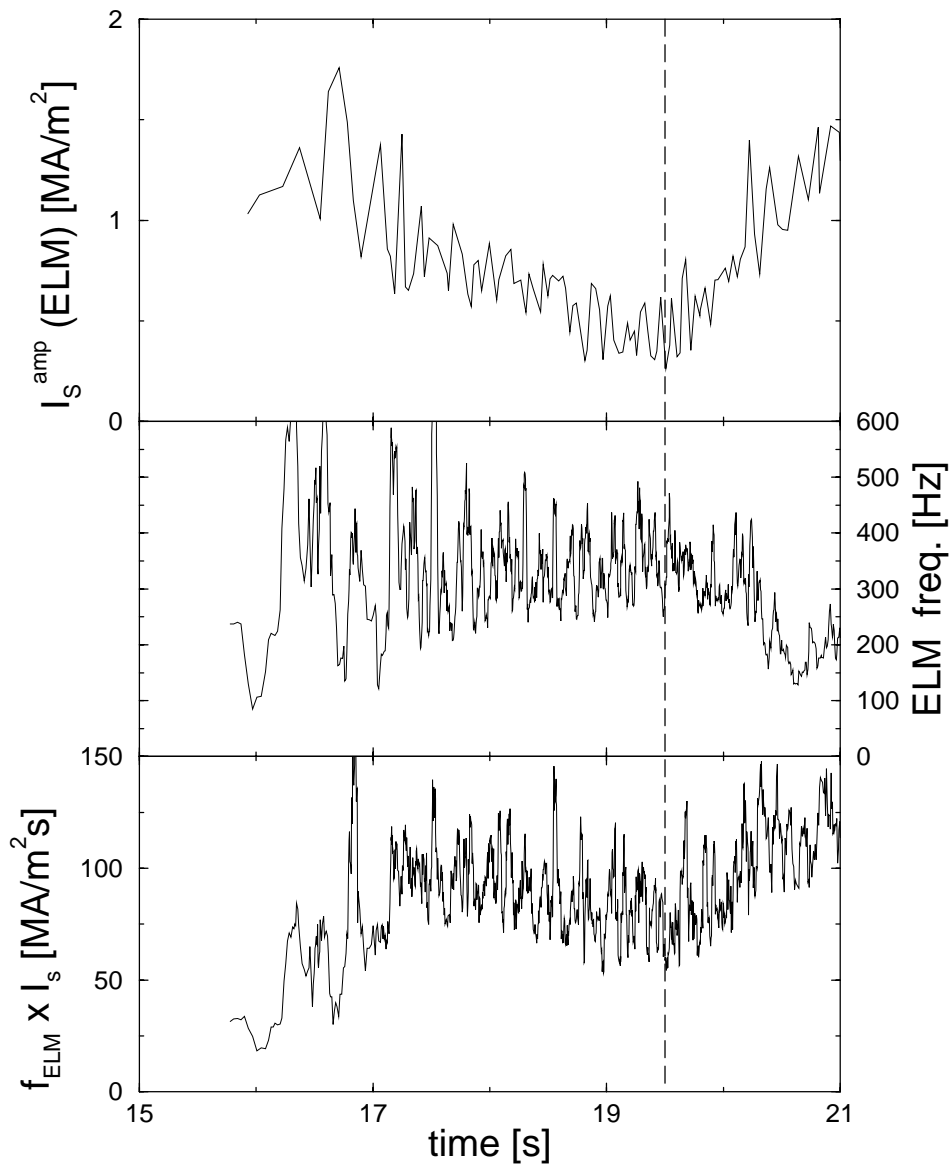


Figure 7. #53318, outer divertor strike zone: Upper envelope of ion saturation current, meaning ELM amplitude; ELM frequency; ELM frequency times the ion saturation current; the vertical dashed line indicates the time of 90% radiative power fraction.

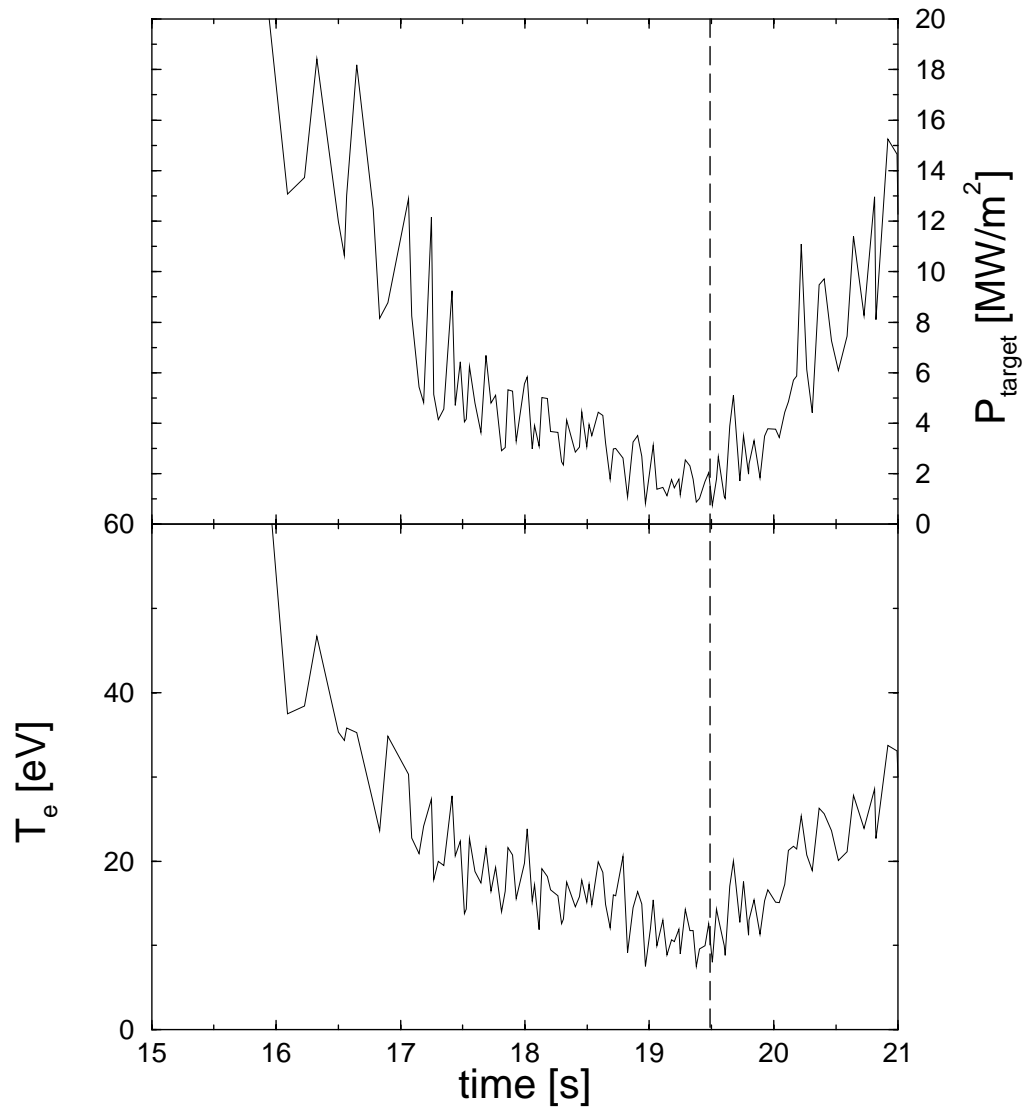


Figure 8. #53318, outer divertor strike zone: target heat flux density as derived from Langmuir probes; electron temperature in-front of the target plate; the vertical dashed line indicates the time of 90% radiative power fraction.

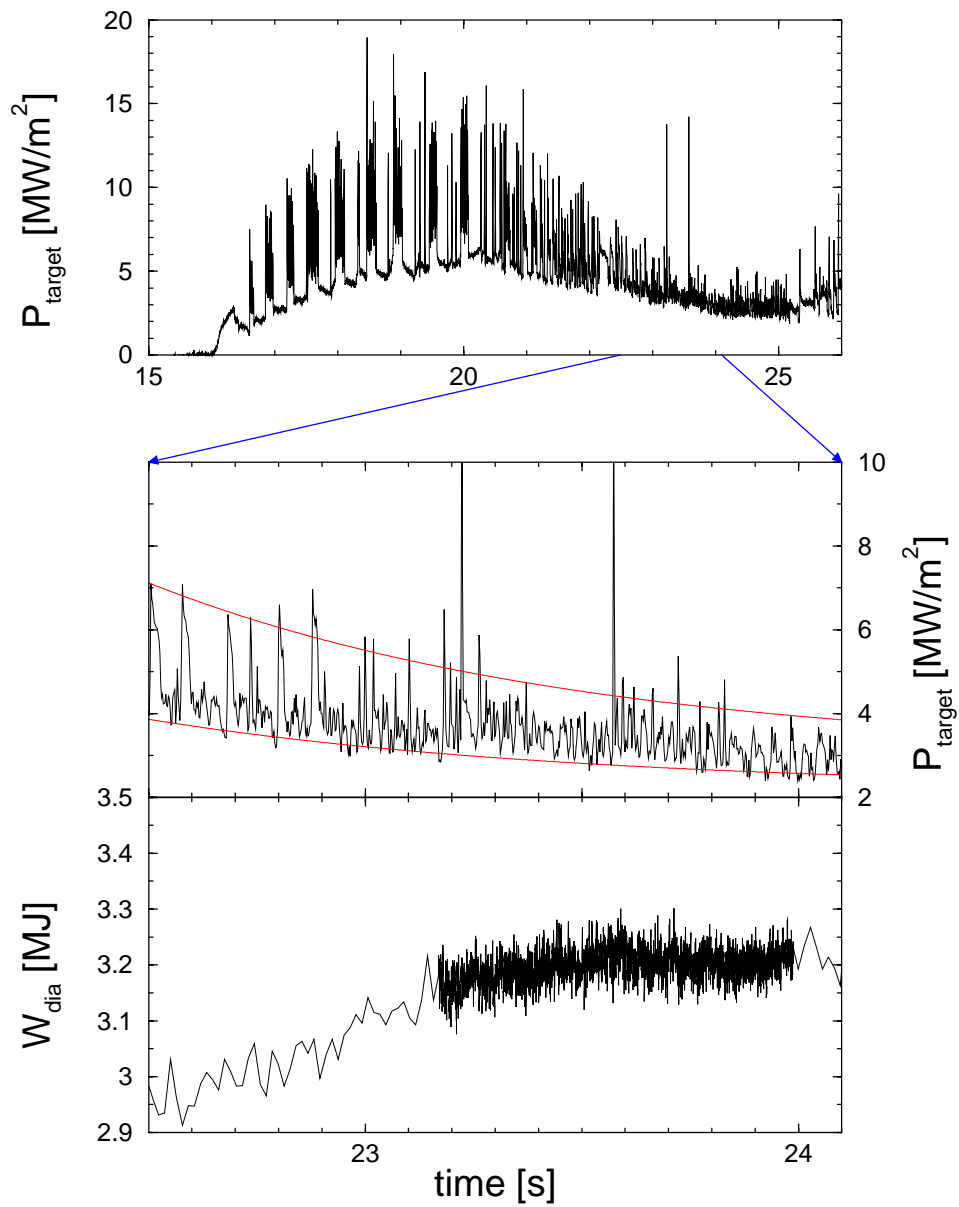


Figure 9. #53772, outer divertor 07 zone: target heat flux density as derived from IR-thermography, the red lines should guide the eyes for an approximate upper and lower envelope; diamagnetic energy, fast sampled between 23.2 and 24 s.

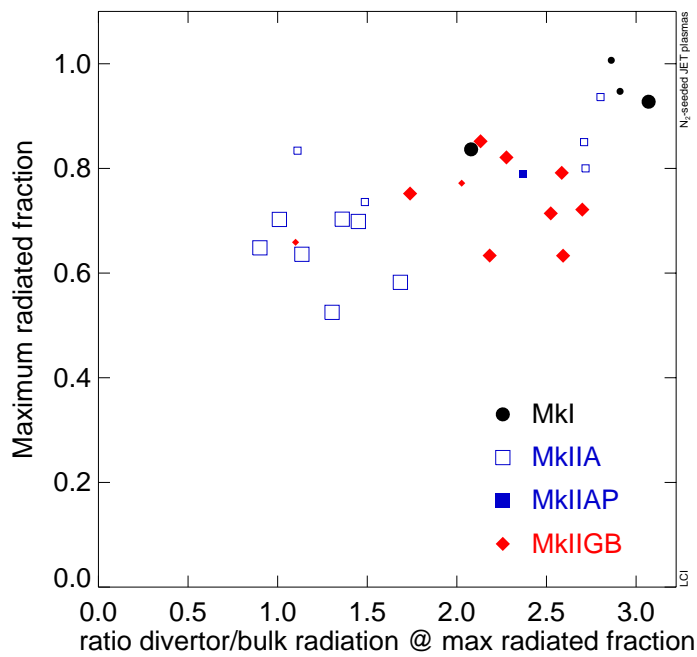


Figure 10. Comparison of the radiative power fractions achieved in JET divertors with nitrogen seeding as function of the ratio of divertor to total radiation: Mk-I, Mk-IIA, Mk-IIAP, Mk-IIGB; small symbols indicate disrupted discharges, where the radiated powers were taken at arbitrary times before the actual disruption.